Journal of Alloys and Compounds 525 (2012) 97–102

Contents lists available at SciVerse ScienceDirect

Journal of Alloys and Compounds

journal homepage: www.elsevier.com/locate/jallcom

Solvothermal synthesis and tailored upconversion emission of monodisperse ultrasmall face-centered cubic Sr_2YF_7 nanocrystals

Mo Ma[a,b], Chang-fu Xu[a,b,*], Li-wen Yang[a,b], Qi-bin Yang[a,b], Jian-guo Lin[a,b]

[a] Key Laboratory of Low Dimensional Materials &Application Technology of Ministry of Education, Xiangtan University, Xiangtan 411105, China
[b] Institute of Modern Physics, Faculty of Material & Photoelectronic Physics, Xiangtan University, Xiangtan 411105, China

ARTICLE INFO

Article history:
Received 15 November 2011
Received in revised form 5 February 2012
Accepted 12 February 2012
Available online xxx

Keywords:
Sr_2YF_7 nanocrystal
Upconversion
Monodisperse
Ultrasmall

ABSTRACT

Monodisperse Sr_2YF_7 nanocrystals with the size of sub-10 nm were synthesized via a solvothermal method by using oleate as a capping ligand. X-ray diffraction and transmission electron microscopy assays reveal that the as-synthesized Sr_2YF_7 nanocrystals are face-centered cubic structure with the cell parameter $a = 5.704$ Å. Intense upconversion luminescence can be observed in Er^{3+}/Yb^{3+} and Tm^{3+}/Yb^{3+} codoped Sr_2YF_7 nanocrystals under the excitation of a 980 nm laser and near-white-color emission can be obtained in $Er^{3+}/Tm^{3+}/Yb^{3+}$ tri-doped Sr_2YF_7 nanocrystals. Energy transfer (ET) from Yb^{3+} to Er^{3+} and Tm^{3+} is mainly responsible to pump Er^{3+} and Tm^{3+} from the ground state to higher states. In $Er^{3+}/Tm^{3+}/Yb^{3+}$ tri-doped Sr_2YF_7 nanocrystals, ET from Tm^{3+} to Er^{3+} leads average three-photon process, which renders the 523 nm emission.

1. Introduction

The advent of new techniques allowing for the facile synthesis of nanosized phosphors has triggered great interests in the research of novel ultrasmall monodisperse light-emitting nanomaterials for their real and potential applications in solid-state lasers, bioimaging and bioseparation, optical data storage and three-dimensional flat-panel display [1–6]. Especially in recent years, uniform and monodisperse upconversion (UC) rare earth (RE) nanocrystals with controllable shapes have attracted considerable devotion because of their applications in bioimaging and fluorescent labels [6–9]. Ultrasmall UC nanocrystals have the potential to substitute quantum dots as staining agents in subcellular level due to their excellent photo-stability, the absence of autofluorescence, and the deep penetration depth of infrared excitation [10–12]. Many series of RE compounds such as fluorides [13–15], oxyfluorides [16], hydroxides [17], vanadates [18], phosphates [19] and oxysulfides [20] reported previously as host nanomaterials, can exhibit highly efficient UC emission. However, just few kinds can keep high UC efficiency when their size is as small as sub-10 nm, so it is essential to search for new type of monodisperse ultrasmall nanocrystals with highly efficient UC emission. Among all of the UC host materials reported to date, β-$NaYF_4$ is recognized as the highest efficient host material. Generally speaking, UC emission efficiency decreases drastically as the size of nanocrystals decreases [21]. However, when the size of nanocrystals is reduced to sub-10 nm, something may be different. Lin et al. [22] had proved that the ultrasmall core/shell $BaGdF_5$ nanocrystals with the size of sub-10 nm possessed higher efficiency of UC emission than β-$NaYF_4$ nanocrystals. Therefore, how to improve the luminescent emission intensity of UC ultrasmall nanocrystals or find novel host nanocrystals with higher luminescent intensity is currently being pursued.

RE fluorides including ReF_3, $LiREF_4$ and $NaREF_4$ have been studied broadly for their low phonon energy and controllable morphology [8,17,23], while there are few reports on other promising host materials, for example, xMF_2-$yREF_3$ nanocrystals. Recently, several uniform monodisperse barium lanthanide fluoride nanocrystals with ultrasmall size such as $BaYF_5$ [24,25], Ba_2YbF_7 [26], $BaGdF_5$ [22,27], Ba_2LaF_7 [28], which possess highly efficient UC emission, had been reported. Furthermore, Ba_2LaF_7 nanocrystals with sub-10 nm present higher UC efficiency than α-$NaYF_4$ nanocrystals with the same size and the same doping conditions [28]. Sr_2YF_7, a ternary compound of fluoride and to the best of our knowledge, has not been synthesized as monodisperse nanocrystals with intense UC emission. In this paper, we will report the solvothermal synthesis of Sr_2YF_7 nanocrystals with the size of sub-10 nm. Intense upconversion emission can be observed in Er^{3+}/Yb^{3+} or Tm^{3+}/Yb^{3+} codoped Sr_2YF_7 nanocrystals and near-white-color emission can be tuned by using $Er^{3+}/Tm^{3+}/Yb^{3+}$ tri-doped Sr_2YF_7 nanocrystals. Especially, Sr_2YF_7 nanocrystals present similar upconversion efficiency with Ba_2LaF_7 [28] and Ba_2YbF_7 [26] nanocrystals under the same doping conditions and the same size. Compared with series of $NaLnF_4$ nanocrystals,

* Corresponding author.
E-mail address: xcf@xtu.edu.cn (C.-f. Xu).

0925-8388/$ – see front matter © 2012 Elsevier B.V. All rights reserved.
doi:10.1016/j.jallcom.2012.02.080

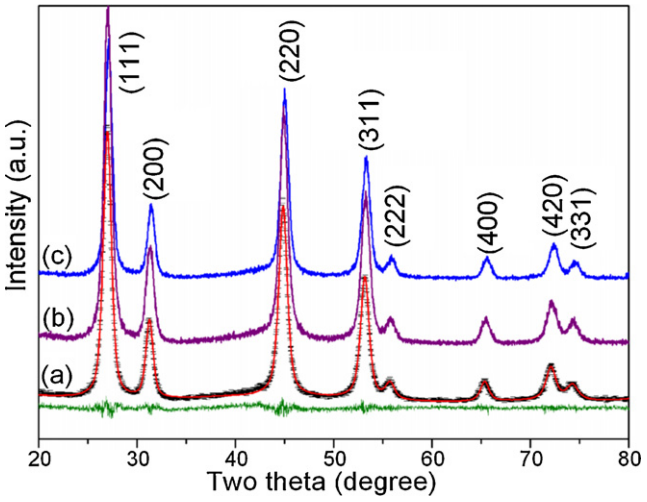

Fig. 1. XRD patterns of the as-synthesized face-centered cubic structure nanocrystals: (a) Sr_2YF_7 (the scattered "–" lines are the raw XRD data and the overlapping red lines are calculated pattern. The olive curves at the bottom are the difference between the raw XRD data and the calculated data); (b) Sr_2YF_7: Yb/Tm (20/0.2 mol%); (c) Sr_2YF_7 (Yb/Er = 20/4 mol%).

Sr_2YF_7 nanocrystals with smaller size have potential applications in bioimaging.

2. Experimental

2.1. Synthesis of Sr_2YF_7 nanocrystals

All reagents were purchased from Sinapharm Chemical Reagent Co, Ltd. and without further purification, but the RE oxides purities are higher than 99.99%. RE oxides were dissolved in nitric acid at elevated temperature to form 0.5 M RE nitride solution, and then $Tm(NO_3)_3$ and $Er(NO_3)_3$ solutions were diluted to 0.05 M. Sr_2YF_7 nanocrystals were synthesized by the following solvothermal method, which was used to synthesize $BaYF_5$, Ba_2YbF_7 and $BaGdF_5$ nanocrystals in our previous reports [26–28]. In a typical synthesis protocol, 2 ml aqueous solution containing 0.6 g NaOH, 10 ml pentanol and 20 ml oleic acid were added into a beaker in turn under stirring to form transparent homogeneous solution. Next, 1.0 mmol $Sr(NO_3)_2$ dissolved in 2 ml deionized water and 0.5 mmol $Y(NO_3)_3$ aqueous solution were introduced into the former solution. At last, 4 mmol NH_4F dissolved in 2 ml deionized water was added in. After another 10 min agitation, the resulting homogeneous colloidal solution was transferred into a 50 ml stainless Teflon-lined autoclave and reacted at 220 °C for 24 h in a furnace. After reaction, the autoclave was moved out from furnace and cooled to room temperature naturally. The products deposited at the bottom of Teflon vessel were collected and washed with ethanol and water several times to remove other remnants, and then dried at 70 °C for 24 h or more time. With these protocols, a series of Er^{3+}/Yb^{3+}, Tm^{3+}/Yb^{3+} codoped and $Er^{3+}/Tm^{3+}/Yb^{3+}$ tri-doped Sr_2YF_7 nanocrystals were synthesized.

2.2. Characterization

The phase and structure were identified by a D/Max 8550 X-ray power diffraction (XRD) apparatus with Cu Kα radiation (λ = 1.5406 nm) at 40 kV and 40 mA. Analysis of XRD data for WPF refinement was performed with MDI Jade 6.0 software. The size, shape and structure of the as-prepared nanocrystals were characterized by transmission electron microscopy (TEM, JEM-2100) at 200 kV equipped with an Oxford instrument energy dispersive X-ray spectroscopy (EDS) system. The samples can be redispersed in cyclohexane under ultrasonication to achieve a well-dispersed suspension, and then one drop of this suspension was dropped on a copper grid covered with hollow carbon film for TEM characterization. UC photoluminescent spectra were recorded by an R-500 fluorescence spectrophotometer under the excitation of an unfocused 980 nm laser. The photoluminescence of lanthanide doped Sr_2YF_7 nanocrystals redispersed in cyclohexane was photographed by a digital camera (Nikon D4000). All of the measurements were performed at room temperature.

3. Results and discussion

3.1. Structure and shape of the as-synthesized nanocrystals

XRD and TEM assays are used to characterize the phase, structure and shape of as-synthesized nanocrystals. Fig. 1 shows

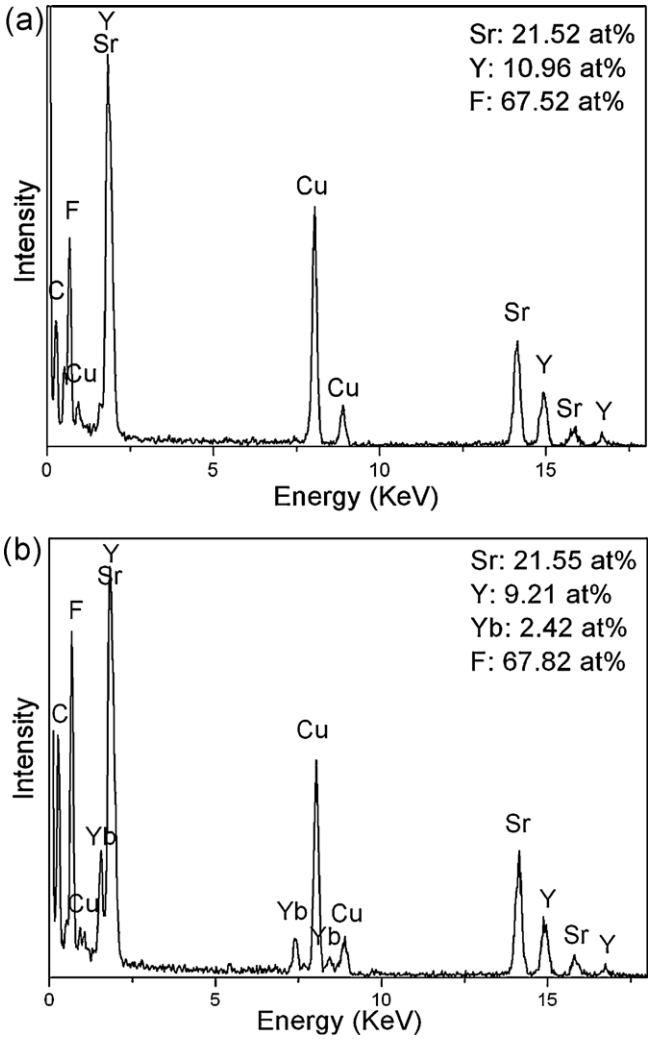

Fig. 2. Energy dispersive X-ray spectroscopy (EDS) analyses of (a) Sr_2YF_7 and (b) Sr_2YF_7 (Yb/Er = 20/4 mol%) nanocrystals.

the typical XRD patterns of the as-synthesized (a) Sr_2YF_7, (b) Sr_2YF_7:Yb/Tm (20/0.2 mol%) and (c) Sr_2YF_7:Yb/Er (20/4 mol%) nanocrystals. Eight characteristic diffraction peaks appear at the positions of 2θ (d-value Å) = 26.95° (3.293), 31.24° (2.852), 44.81° (2.017), 53.12° (1.720), 55.69° (1.647), 65.30° (1.426), 72.03° (1.309) and 74.22° (1.276) on the XRD pattern of Sr_2YF_7 (Fig. 1(a)), respectively. According to the equation $r^{*2} = 1/d^2$, where r^* is the length of reciprocal vector and d is the lattice fringe of diffraction peak, $r_1^* : r_2^* : r_3^* : r_4^* : r_5^* : r_6^* : r_7^* : r_8^*$ value of Sr_2YF_7 is very close to 3:4:8:11:12:16:19:20, so the phase structure of the as-synthesized nanocrystals can be determined to be face-centered cubic structure.

EDS analysis was performed to measure the compositions of the undoped and Yb^{3+}/Er^{3+} (20/4 mol%) codoped Sr_2YF_7 nanocrystals and the results are shown in Fig. 2. Besides the copper and the carbon come from the copper grid and oleate ligands capped on the surface of nanocrystals, the atom contents of Sr, Y and F for the undoped nanocrystals (shown in Fig. 2(a)) are 21.52, 10.96 and 67.52 at%, respectively, which are close to the formula of Sr_2YF_7 when EDS measurement error was considered. Fig. 2(b) reveals the atom contents of Sr, Y, Yb and F for the Yb^{3+}/Er^{3+} (20/4 at%) codoped nanocrystals are 21.55, 9.21, 2.42 and 67.82 at%, respectively, which further confirms the formula of Sr_2YF_7. Moreover, the XRD data of the as-synthesized undoped nanocrystals were processed with Jade 6.0 software for WPF refinement. The calculated results and

the XRD data, as well as the difference between them, are given in Fig. 1(a). It can be seen that the calculated value are in good agreement with the XRD data with the difference of $R = 10.28\%$. Therefore, it is believable that the as-synthesized Sr_2YF_7 nanocrystals are of face-centered cubic structure (space group: $Fm\bar{3}m$) with the cell parameters $a = 5.704$ Å. The diffraction peaks of the Yb^{3+}/Tm^{3+} and Yb^{3+}/Er^{3+} codoped nanocrystals shift very little to the right because the radius of Yb^{3+} is smaller than that of Y^{3+}.

The widening of diffraction peaks confirms that the as-synthesized nanocrystals are of ultrasmall size. The average size of the as-synthesized nanocrystals can be estimated by Scherrer equation: $D = K\lambda/\beta\cos\theta$, where λ is the X-ray wavelength (0.15406 nm), β is the full-width at half-maximum, θ is the Bragg angle, and K is a constant (0.89). The average sizes, which are calculated with β-value of (1 1 1) peak, can be estimated to be 8.6 nm for the undoped Sr_2YF_7, 9.5 nm for Tm^{3+}/Yb^{3+} codoped Sr_2YF_7 (Yb/Tm = 20/0.2 mol%) and 8.9 nm for Er^{3+}/Yb^{3+} codoped Sr_2YF_7 (Yb/Er = 20/4 mol%), respectively.

The cubic structure of the as-synthesized nanocrystals was further confirmed by TEM assay. Fig. 3 provides the low magnification TEM images, high resolution transmission electron microscopy (HRTEM) images and the electron diffraction pattern of the as-synthesized (a) Sr_2Yf_7 and (b) Sr_2YF_7 (Yb/Er = 20/4 mol%) nanocrystals. All of nanocrystals are highly uniform, well dispersed and self-assembled into two-dimensional (2D) array. HRTEM images reveal that the interplanar distances are 2.88 Å corresponding to the (2 0 0) planes of Sr_2YF_7 and 3.28 Å corresponding to the (1 1 1) planes of Sr_2YF_7 (Yb/Er = 20/4 mol%), respectively. Obviously, high concentration doping of Yb^{3+} affects the size and shape of nanocrystals very little. The interplanar distances of Sr_2YF_7 nanocrystals calculating from the inner eight SEAD rings (inset in Fig. 3(a) and only half shown) are 3.30, 2.86, 2.02, 1.71, 1.65, 1.40, 1.32 and 1.28 Å, which can be assigned to {1 1 1}, {2 0 0}, {2 2 0}, {3 1 1}, {2 2 2}, {4 0 0}, {3 3 1} and {4 2 0} lattice planes of the face-centered cubic structure Sr_2YF_7, respectively.

3.2. Upconversion emission of the as-synthesized Sr_2YF_7 nanocrystals

Intense UC emission can be observed in Ln^{3+} (Ln = Er, Tm, Yb) doped Sr_2YF_7 nanocrystals by naked eyes, and the emission color can be tuned by definitely controllable doping. Fig. 4 provides UC spectra of Sr_2YF_7 nanocrystals with different doping conditions under the excitation of an unfocused 980 nm laser with the spot size of 8 mm^2. Two emission bands (Fig. 4(a)), which centered at 523/544 and 654 nm and can be ascribed to $^2S_{11/2}/^4H_{3/2} \rightarrow {}^4I_{15/2}$ and $^4F_{9/2} \rightarrow {}^4I_{15/2}$ transitions of Er^{3+}, lead to yellow color emission (as shown in Fig. 4(a)). The integrated intensity ratio of red to green (R/G) varied with the Er^{3+} doping concentration. In addition, when the Er^{3+} doping concentration decreased from 10 mol% to 4 mol%, not only the emission intensity decreased, but also R/G varied from 2.003 to 0.884. For comparison, the upconversion spectra of Ba_2LaF_7 (Yb/Er = 20/4 mol%) nanocrystals [28] with similar size were shown in Fig. 4(a)(iii). Intensity UC from the ultraviolet to the near-infrared was obtained in Tm^{3+}/Yb^{3+} doped Sr_2YF_7 nanocrystals. Fig. 4(b) shows UC spectra of Sr_2YF_7:Yb/Tm (20/0.2 mol%) which consist of four emission bands. The ultraviolet emission can be ascribed to $^1I_6 \rightarrow {}^3F_4/^1D_2 \rightarrow {}^3H_6$ transitions of Tm^{3+} (centered at 347 and 361 nm). The intense blue emission is originated from $^1D_2 \rightarrow {}^3F_4$ and $^1G_4 \rightarrow {}^3H_6$ transitions of Tm^{3+} (centered at 452 and 478 nm). The transitions of $^1G_4 \rightarrow {}^3F_4$, $^3F_3 \rightarrow {}^3H_6$ and $^3F_2 \rightarrow {}^3H_6$ (centered at 649, 700 and 724 nm, respectively) lead to weakly visible red emission, while the $^3H_4 \rightarrow {}^3H_6$ transition of Tm^{3+} (centered at 773 and 803 nm) makes the dominated infrared emission. The near-white-color emission can be easily tailored by $Er^{3+}/Tm^{3+}/Yb^{3+}$ tri-doped Sr_2YF_7 nanocrystals (Fig. 4(c)) [25]. Sr_2YF_7 nanocrystals can be easily redispersed in cyclohexane to form transparent colloidal solution, which can realize intense UC emission under the excitation of the 980 nm laser. Insets in Fig. 4(a)–(c) shows the digital photographs taken from the colloidal solution under the excitation of a 980 nm laser (40 W/cm^2), and intense UC can be seen from the photographs.

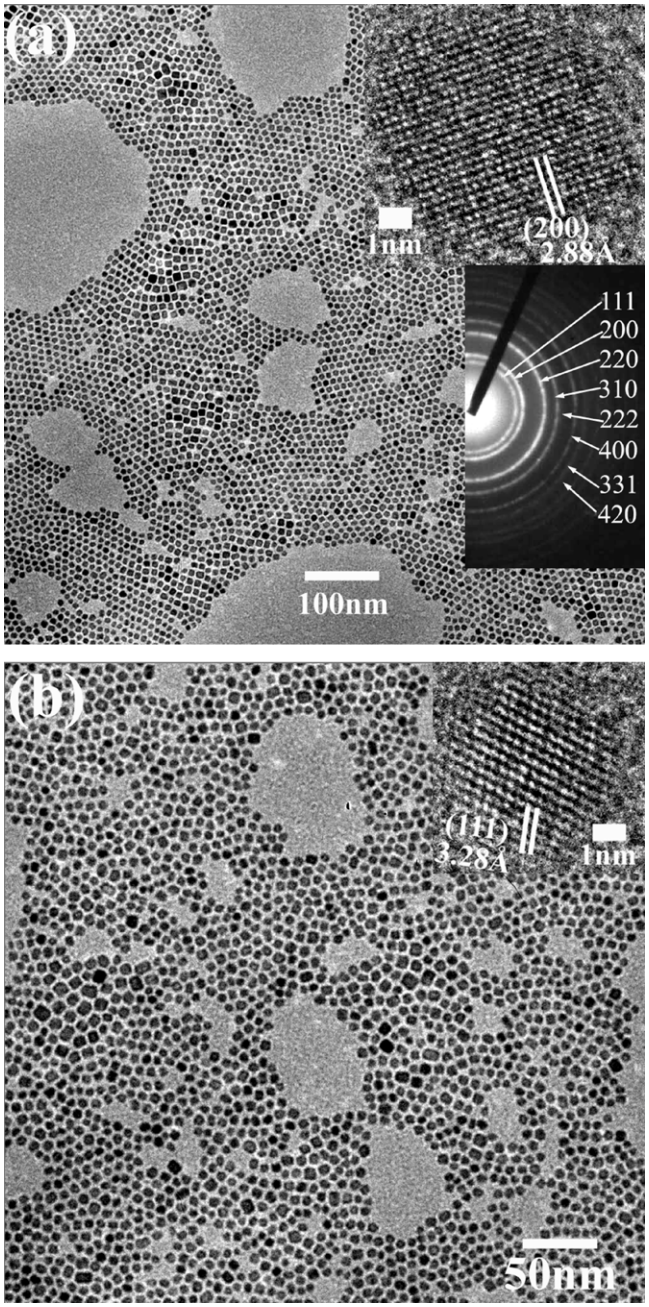

Fig. 3. TEM images of (a) undoped Sr_2YF_7 and (b) Sr_2YF_7 (Yb/Er = 20/4 mol%) nanocrystals with the corresponding HRTEM images inset in the upper right.

To clarify UC emission mechanism of Er^{3+}/Yb^{3+} and Tm^{3+}/Yb^{3+} codoped Sr_2YF_7, the dependence of emission intensity I_{up} from Sr_2YF_7 nanocrystals on the infrared excitation power P were measured and shown in Fig. 5. The relationship between the intensity of UC luminescence I_{up} and the pump power P can be written as: $I_{up} \propto P^N$, where N is the order of multi-photon transitions, the number of infrared quanta absorbed per photon emission. From the inset in Fig. 5(a), we can see that the values of N for sample

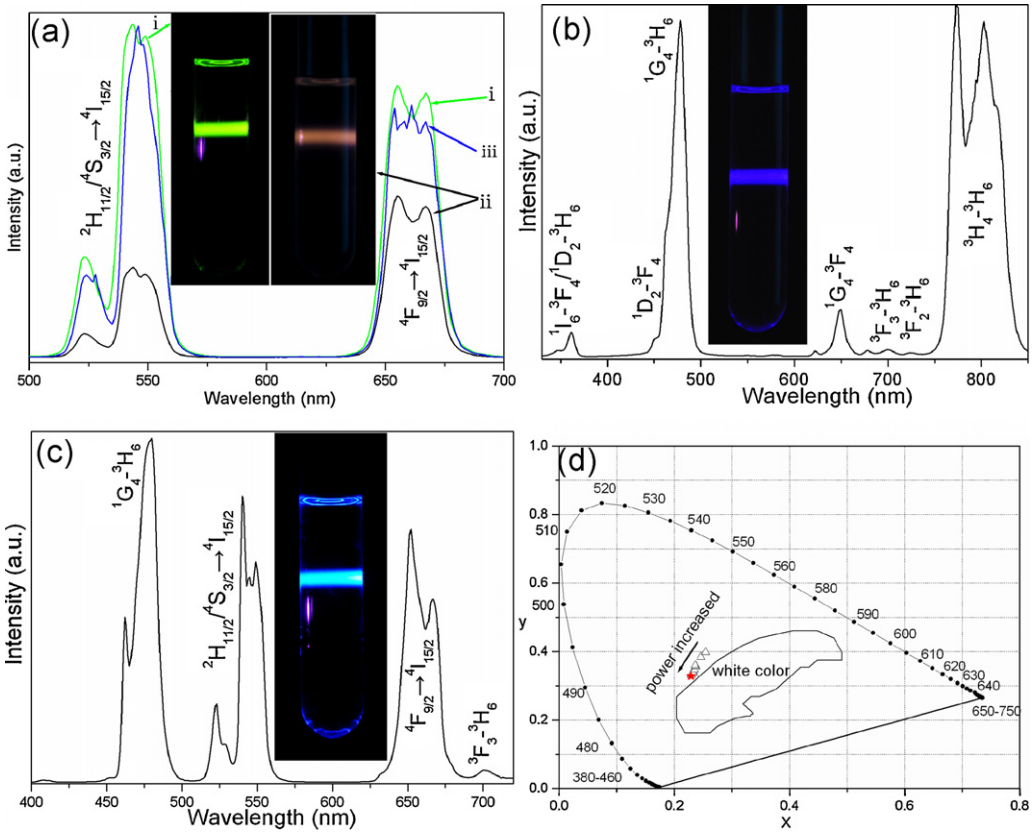

Fig. 4. Upconversion spectra of Sr_2YF_7 nanocrystals with different doping conditions under the excitation of the 980 nm laser and their corresponding digital photographs: (a) (i) Sr_2YF_7 (Yb/Er = 20/10 mol%), (ii) Sr_2YF_7 (Yb/Er = 20/4 mol%) and (iii) Ba_2LaF_7 (Yb/Er = 20/4 mol%); (b) Sr_2YF_7:Yb/Tm (20/0.2 mol%); (c) Sr_2YF_7:Yb/Er/Tm (20/0.3/0.4 mol%) with its (d) CIE diagram (the spectra of c is marked with "⋆") under different excitation power.

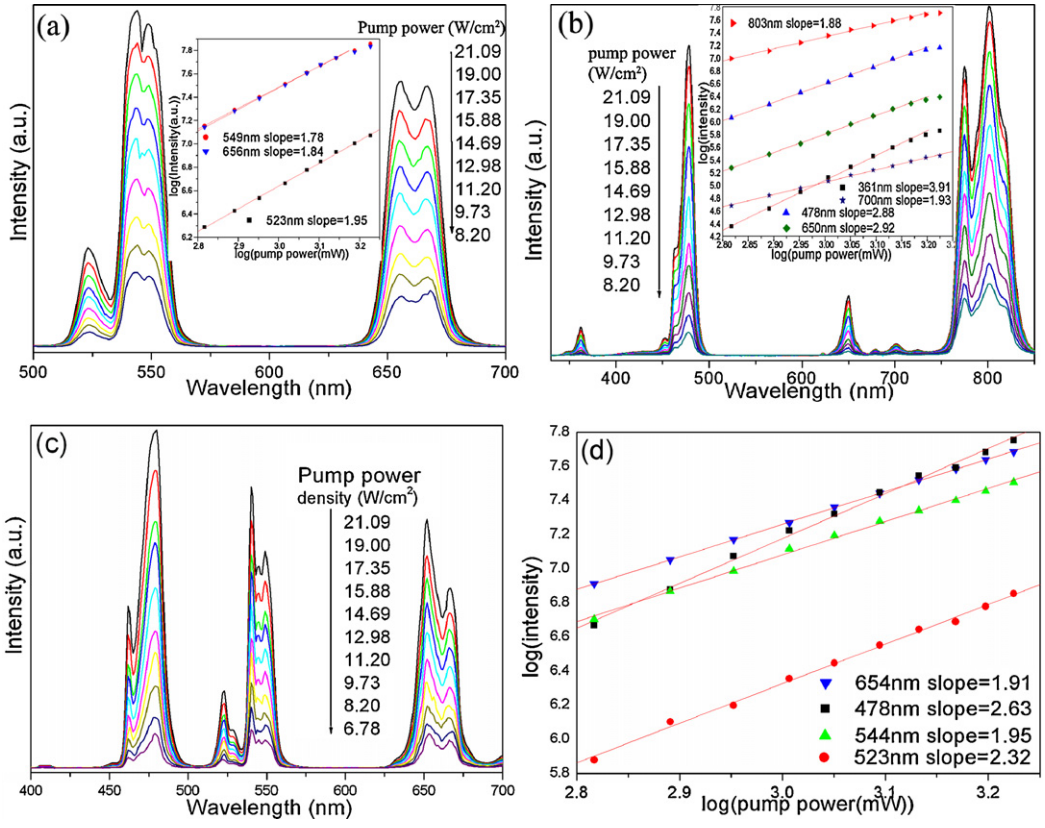

Fig. 5. Upconversion spectra of (a) Sr_2YF_7 (Yb/Er = 20/10 mol%), (b) Sr_2YF_7:Yb/Tm (20/0.2 mol%) and (c) Sr_2YF_7:Yb/Er/Tm (20/0.3/0.4 mol%) under the excitation of an unfocused 980 nm laser with different pump power densities. The insets in each image and (d) are the corresponding double-logarithm plots of the upconversion emission intensity versus the pump power densities.

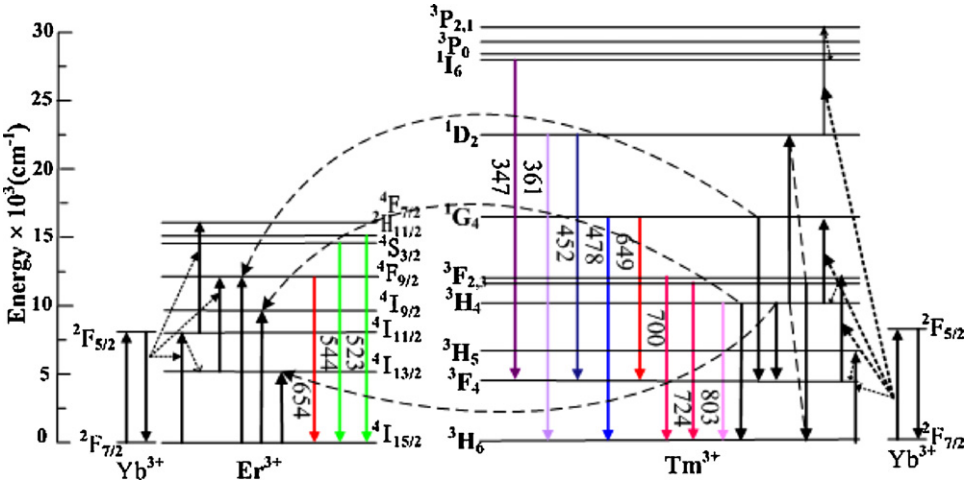

Fig. 6. Schemes of energy transfer processes of $Yb^{3+} \rightarrow Er^{3+}$, $Yb^{3+} \rightarrow Tm^{3+}$ and $Tm^{3+} \rightarrow Er^{3+}$, and the proposed upconversion mechanisms of the tailored-color emission of Er^{3+}/Yb^{3+}, Tm^{3+}/Yb^{3+} codoped and $Er^{3+}/Tm^{3+}/Yb^{3+}$ tri-doped Sr_2YF_7 nanocrystals under the excitation of an unfocused 980 nm laser.

Sr_2YF_7 (Yb/Er = 20/10 mol%) are 1.95, 1.78 and 1.84 at 523, 549 and 656 nm emissions, indicating 2 photons needed to realize the transitions of $^2S_{11/2}/^4H_{3/2} \rightarrow {}^4I_{15/2}$ and $^4F_{9/2} \rightarrow {}^4I_{15/2}$. The inset in Fig. 5(b) indicates that the slope values of the linear fits with the experimental data are 3.91, 2.88, 2.92, 1.93 and 1.88 for the five observed UC emission bands. These results reveal that 4, 3, 3, 2 and 2 photons are necessary to realize UC emissions centered at 361, 478, 650, 700 and 803 nm, which are consistent with other previous reports in Tm^{3+}/Yb^{3+} codoped $BaGdF_5$, $BaYF_5$ and Tm^{3+} doped Ba_2YbF_7 nanocrystals [26–29]. In addition, the slope values for each emission bands tend to decrease with the increase of pump power intensity, which may be originated from the saturation effect [30–32]. As the pump power increases to certain intensity, the absorption of Yb^{3+} gets saturated. Another reason may be related to the excited states of Er^{3+} ($^4I_{11/2}$) and Tm^{3+} ($^3F_4$) owing to the efficient energy transfer (ET) processes from Yb^{3+} to Er^{3+} or Tm^{3+}, which result in the following ET processes populating the upper excited states so efficient that it exceeds the spontaneous decay rate to the ground state [31,32].

Auzel had extensively discussed UC mechanisms of the 4f electron levels of rare earth ions in different matrices [1]. The energy level diagrams of Er^{3+}, Tm^{3+} and Yb^{3+} are shown in Fig. 6 which has indicated the possible UC mechanisms to produce the tailored-color UC emission. For Yb^{3+} has much bigger absorption section than Er^{3+} or Tm^{3+} under the excitation of the 980 nm laser, high efficient UC processes of Er^{3+}/Yb^{3+} or Tm^{3+}/Yb^{3+} codoped Sr_2YF_7 nanocrystals are mainly originated from the sensitization of Yb^{3+} ions [33]. As shown in Fig. 6, Er^{3+} is pumped to $^4I_{11/2}$ level by ET from Yb^{3+}, and then partly nonradiatively relaxes to next lower level $^4I_{13/2}$. The successive ET from Yb^{3+} forms the populations of $^4F_{7/2}$ and $^4F_{9/2}$ levels (Er^{3+}). The electrons populated on $^4F_{7/2}$ level nonradiatively relax to next lower levels $^2H_{11/2}$ and $^4S_{3/2}$. So the green and red emission bands are originated from the electron transitions from the $^2H_{11/2}$, $^4S_{3/2}$ and $^4F_{9/2}$ levels to the ground state. The possible UC mechanisms of Tm^{3+}/Yb^{3+} codoped Sr_2YF_7 nanocrystals might be realized via the multiple phonon-assisted energy transfer processes from Yb^{3+} ions to Tm^{3+} ions as follows: $^2F_{5/2}$ (Yb^{3+}) + $^3H_6$ (Tm^{3+}) → $^3H_5$ (Tm^{3+}) + $^2F_{7/2}$ (Yb^{3+}) ~ $^3F_4$ (Tm^{3+}) + multiphonon relaxation, $^2F_{5/2}$ (Yb^{3+}) + $^3F_4$ (Tm^{3+}) → $^3F_2/^3F_3$ (Tm^{3+}) + $^2F_{7/2}$ (Yb^{3+}) ~ $^3H_4$ (Tm^{3+}) + multiphonon relaxation, $^2F_{5/2}$ (Yb^{3+}) + $^3H_4$ (Tm^{3+}) → $^1G_4$ (Tm^{3+}) + $^2F_{7/2}$ (Yb^{3+}), $^3H_4$ (Tm^{3+}) + $^3F_3$ (Tm^{3+}) → $^1D_2$ (Tm^{3+}) + $^3H_6$ (Tm^{3+}), $^2F_{5/2}$ (Yb^{3+}) + $^1D_2$ (Tm^{3+}) → $^3P_{1,2}$ (Tm^{3+}) + $^2F_{7/2}$ (Yb^{3+}) ~ $^1I_6$ (Tm^{3+}) + multiphonon relaxation [15]. Then, the transitions from the excited state levels to lower and ground states lead the emissions of Tm^{3+} centered at 347, 361, 452, 478, 649, 700, 724 and 803 nm, respectively.

The near-white-color emission of Sr_2YF_7 (Yb/Er/Tm = 20/0.3/0.4 mol%) nanocrystals is shown in Fig. 5(c) and (d) and its CIE diagrams under different excitation power are presented in Fig. 4(d) (marked with Δ). The slope values of the fitting lines are 2.63, 2.32, 1.95 and 1.91, which indicate 3, 3, 2 and 2 photons are needed to realize the emission centered at 478, 523, 544 and 654 nm, respectively. It is noticed that the emission of $Er^{3+}/Tm^{3+}/Yb^{3+}$ tri-doped Sr_2YF_7 nanocrystals centered at 523 nm, which is different from that of Er^{3+}/Yb^{3+} codoped Sr_2YF_7 nanocrystals. For tri-doped nanocrystals, it is three-photon process to populate the $^2H_{11/2}/^4S_{3/2}$ [34,35], but two-photon process for Er^{3+}/Yb^{3+} codoped nanocrystals. In our experiment, the mechanism to realize the 523 nm emission that we suppose is different from other's reports [33,34]. In addition, the ultraviolet emission is hardly detected in tri-doped Sr_2YF_7 nanocrystals, which means that ET from Tm^{3+} to Er^{3+} occurs. As shown in Fig. 6, three processes can transfer the energy from Tm^{3+} to Er^{3+} as following: $^3H_4$ (Tm^{3+}) + $^4H_{15/2}$ (Er^{3+}) → $^3H_6$ (Tm^{3+}) + $^4F_{9/2}$ (Er^{3+}), $^1G_4$ (Tm^{3+}) + $^4H_{15/2}$ (Er^{3+}) → $^3F_4$ (Tm^{3+}) + $^4I_{9/2}$ (Er^{3+}), $^3H_4$ (Tm^{3+}) + $^4H_{15/2}$ (Er^{3+}) → $^3F_4$ (Tm^{3+}) + $^4H_{13/2}$ (Er^{3+}). Multi-photons are needed to pump Tm^{3+} to higher energy levels and at least one photon is needed to pump Er^{3+} from the excited state to $^4F_{7/2}$ or $^4H_{9/2}$, so average three photons are needed to realize the 523 nm emission of Er^{3+}.

4. Conclusion

Monodisperse ultrasmall Sr_2YF_7 nanocrystals with the size of sub-10 nm were synthesized via solvothermal method by using oleate as capping ligands. XRD and TEM assays reveal that the as-synthesized Sr_2YF_7 nanocrystals are of face-centered cubic structure with the cell parameter of 5.704 Å. Intense UC can be observed in Er^{3+}/Yb^{3+} and Tm^{3+}/Yb^{3+} codoped Sr_2YF_7 nanocrystals and near-white-color emission can be obtained in definitely controlled $Er^{3+}/Tm^{3+}/Yb^{3+}$ tri-doped Sr_2YF_7 nanocrystals. The main mechanism of UC emission is ET. ET from Tm^{3+} to Er^{3+} leads to the decrease of ultraviolet and blue emission intensity of Tm^{3+} and the increase of green emission intensity of Er^{3+}, which renders average three-photon process to realize the 523 nm emission and ascribed to the white UC emission.

References

[1] F. Auzel, Chem. Rev. 104 (2004) 139.
[2] H.S. Mader, P. Keke, S.M. Saleh, O.S. Wolfbeis, Curr. Opin. Cell Biol. 14 (2010) 582.
[3] D.K. Chatterjee, M.K. Gnanasammandhan, Y. Zhang, Small 6 (2010) 2781.
[4] M. Nyk, T.R. Kumar, T.Y. Ohulchanskyy, E.J. Bergey, P.N. Prasad, Nano Lett. 8 (2002) 3834.
[5] A. Patra, C.S. Friend, R. Kapoor, P.N. Prasad, Appl. Phys. Lett. 83 (2003) 284.
[6] F. Wang, Y. Han, C.S. Lim, Y.H. Lu, J. Wang, J. Xu, H.Y. Chen, C. Zhang, M.H. Hong, X.G. Liu, Nature 463 (2010) 1061.
[7] D. Chen, Y. Yu, F. Huang, P. Huang, A. Yang, Y.S. Wang, J. Am. Chem. Soc. 132 (2010) 9976.
[8] G.Y. Chen, T.Y. Ohulchanskyy, R. Kumar, H. Ågren, P.N. Prasad, ACS Nano 4 (2010) 3163.
[9] F. Wang, X.G. Liu, Chem. Soc. Rev. 38 (2009) 976.
[10] X.Y. Wu, H.J. Liu, J.Q. Liu, K.N. Haley, J.A. Treadway, J.P. Larson, N.F. Ge, G. Peale, M.P. Bruchez, Nat. Biotechnol. 21 (2003) 41.
[11] L. Xiong, T. Yang, Y. Yang, C. Xu, F.Y. Li, Biomaterials 31 (2010) 7078.
[12] Y. Park, J. Kim, K. Lee, K. Jeon, H. Na, J. Yu, H. Kim, N. Lee, S. Choi, S. Baik, H. Kim, S. Park, B. Park, Y. Kim, S. Lee, S. Yoon, I. Song, W. Moom, Y. Suh, T. Hyeon, Adv. Mater. 21 (2009) 4467.
[13] B. Dubertret, P. Skourides, D.J. Norris, V. Noireaux, A.H. Brivanlou, A. Libchaber, Science 298 (2002) 1759.
[14] C. Li, J. Yang, P. Yang, H. Lian, J. Lin, Chem. Mater. 20 (2008) 4317.
[15] F. Wang, R.R. Deng, J. Wang, Q.X. Wang, Y. Han, H.M. Zhu, X.Y. Chen, X.G. Liu, Nat. Mater. 10 (2011) 968.
[16] X. Sun, Y. Zhang, Y. Du, Z. Yan, R. Si, L. You, C. Yan, Chem. Eur. J. 13 (2007) 2320.
[17] Q. Zhang, B. Yan, Inorg. Chem. 49 (2010) 6834.
[18] X. Wang, Y. Li, Angew. Chem. Int. Ed. 41 (2002) 4790.
[19] J.W. Stouwdam, M. Raudsepp, F.C.J.M. Veggel, Langmuir 21 (2005) 7003.
[20] Z. Huo, C. Chen, D. Chu, H. Li, Y. Li, Chem. Eur. J. 13 (2007) 7708.
[21] A.X. Yin, Y.W. Zhang, L.D. Sun, C.H. Yan, Nanoscale 2 (2010) 953.
[22] D.M. Yang, C.X. Li, G.G. Li, M.M. Shang, X.J. Kang, J. Lin, J. Mater. Chem. 21 (2011) 5923.
[23] F. Zhang, D.Y. Zhao, ACS Nano 3 (2009) 159.
[24] F. Wang, X.G. Liu, J. Am. Chem. Soc. 130 (2008) 5642.
[25] Y. Huang, H. You, G. Jia, Y. Song, Y. Zheng, M. Yang, K. Liu, N. Guo, J. Phys. Chem. C 114 (2010) 18051.
[26] M. Ma, L. Yang, G. Ren, C.F. Xu, J. Liu, Q. Yang, J. Lumin. 7 (2011) 1482.
[27] C.F. Xu, M. Mo, L. Yang, Q. Yang, J. Lumin. 131 (2011) 2544.
[28] C.F. Xu, M. Ma, L.W. Yang, S.J. Zeng, Q.B. Yang, J. Colloid Interface Sci. 368 (2012) 49.
[29] C.F. Xu, M. Ma, S. Zeng, G. Ren, L. Yang, Q. Yang, J. Alloys Compd. 509 (2011) 7493.
[30] C. Jacinto, M.V.D. Vermelho, E.A. Gouveia, M.T. de Aroujo, P.T. Udo, N.G.C. Astrath, M.L. Baesso, Appl. Phys. Lett. 91 (2007) 071102.
[31] F. Vetrone, V. Mahalingam, J.A. Capobianco, Chem. Mater. 21 (2009) 1847.
[32] L.W. Yang, H.L. Han, Y.Y. Zhang, J.X. Zhong, J. Phys. Chem. C 113 (2009) 18995.
[33] P. Jenouvrier, G. Boccardi, J. Fick, A.M. Jurdyc, M. Langlet, J. Lumin. 113 (2005) 291.
[34] G.Y. Chen, Y. Liu, Y.G. Zhang, G. Somesfalean, Z.G. Zhang, Appl. Phys. Lett. 91 (2007) 133103.
[35] F. Vetrone, J.C. Boyer, J.A. Capobianco, J. Appl. Phys. 96 (2004) 661.